

Statistical reconstruction of two-phase random media



J.W. Feng^a, C.F. Li^{a,*}, S. Cen^{b,c}, D.R.J. Owen^a

^a Civil & Computational Engineering Centre, College of Engineering, Swansea University, United Kingdom

^b Department of Engineering Mechanics, School of Aerospace, Tsinghua University, Beijing, China

^c Key Laboratory of Applied Mechanics, School of Aerospace, Tsinghua University, Beijing, China

ARTICLE INFO

Article history:

Received 20 July 2012

Accepted 24 March 2013

Available online 25 April 2013

Keywords:

Composite material
Random microstructure
Sample reconstruction
Non-Gaussian field
FFT

ABSTRACT

A robust and efficient algorithm is proposed to reconstruct two-phase composite materials with random morphology, according to given samples or given statistical characteristics. The new method is based on nonlinear transformation of Gaussian random fields, where the correlation of the underlying Gaussian field is determined explicitly rather than through iterative methods. The reconstructed media can meet the binary-valued marginal probability distribution function and the two point correlation function of the reference media. The new method, whose main computation is completed using fast Fourier transform (FFT), is highly efficient and particularly suitable for reconstructing large size random media or a large number of samples. Its feasibility and performance are examined through a series of practical examples with comparisons to other state-of-the-art methods in random media reconstruction.

© 2013 Elsevier Ltd. All rights reserved.

1. Introduction

Multi-phase random media such as rocks, concrete, alloy and composite materials are ubiquitous in the natural environment and engineering. Their mechanical, thermal and electrical etc. properties exhibit a strong random nature with discontinuities on the interfaces between different phases. The responses of multi-phase random media subjected to force, thermal or other type of loading are often of great interest to engineers and researchers, and such responses should be analyzed in the sense of statistics due to the inherent heterogeneity. At present, Monte Carlo methods remain the most popular and versatile approach for simulating the randomness of multi-phase random media and estimating their stochastic responses. The effectiveness of Monte Carlo methods relies largely on rapid reconstruction of large amounts of samples that can accurately represent the diversity and variation of the practical random media under simulation.

The main focus of this work is on the reconstruction of two-phase composite materials with random morphology, based on statistical characteristics derived from a few measured samples. The proposed reconstruction method is general and applicable to other types of random media as well, and instead of using the term “composite”, we will use the general term “random media” for the remainder of the paper.

For a two-phase (black & white) random medium D , the indicator function $I(\mathbf{x})$, $\forall \mathbf{x} \in D$ is defined as

$$I(\mathbf{x}) = \begin{cases} 0, & \text{if the material at } \mathbf{x} \text{ is in black phase} \\ 1, & \text{if the material at } \mathbf{x} \text{ is in white phase} \end{cases} \quad (1)$$

Due to the random nature of phase distribution, the indicator function is often treated in the context of probability as a binary valued random field, denoted by $I(\mathbf{x}, \omega)$ where ω indicates a basic random event.

In practice, the random field $I(\mathbf{x}, \omega)$ is often assumed to be stationary (also termed as statistically homogeneous in [1–3]) up to the second order, so that its mean μ and variance σ^2 are invariant when shifted in space. In addition, the autocorrelation function between points \mathbf{x} and $\mathbf{x} + \boldsymbol{\tau}$ depends only on the relative position $\boldsymbol{\tau}$ of the two points, i.e.

$$R_I(\boldsymbol{\tau}) = \frac{E[(I(\mathbf{x}, \omega) - \mu)(I(\mathbf{x} + \boldsymbol{\tau}, \omega) - \mu)]}{\sigma^2}, \quad \forall \mathbf{x}, \quad (2)$$

where $E(\cdot)$ is the expectation operator. The range of $R_I(\boldsymbol{\tau})$ is $-1 \leq R_I(\boldsymbol{\tau}) \leq 1$ (Schwarz inequality).

Another assumption of $I(\mathbf{x}, \omega)$ is ergodicity. That is, the ensemble average of statistical parameters can be derived by the space average of these parameters over a sufficiently large sample.

Given a few, or even only one, realizations of the random media, the task of reconstruction is to extract statistical parameters (μ , σ^2 and $R_I(\boldsymbol{\tau})$ etc.) regarding the random field $I(\mathbf{x}, \omega)$ and generate samples that obey the same statistics as the reference realizations.

2. Overview

2.1. Related work

Over the past few decades, random media reconstruction has attracted growing attention from both academia and industry, in

* Corresponding author. Tel.: +44 (0) 1792 602256; fax: +44 (0) 1792 295676.
E-mail address: c.f.li@swansea.ac.uk (C.F. Li).

particular in the fields of composite materials, geostatistics and computational mechanics. To date, there are four main categories of reconstruction methods: the random set method, the stochastic optimization method, the maximum entropy method and the iterative nonlinear transformation method.

The random set method [4–6] is based on Boolean operations (union, intersection, dilation, erosion, et al. [7]) of random sets. This method is fast but it is limited to a few types of random media with relatively simple morphology, e.g. composites with sphere or polygon inclusions or Voronoi cell structure. For example, if the inclusion phase is spheres, their centers can be generated following a Poisson distribution; the radius can be similarly assumed to obey certain probability distribution; and adjacent spheres need to be trimmed if they overlap. However, for composites with complicated structures, e.g. amorphous phases, the random set objects are difficult to locate and operate, leading to deterioration in efficiency. In short, the random set method is fast and effective for certain types of random media, but is not a universal method.

Yeong and Torquato [1,8] introduced a simulated annealing method for generating digitalized random media realizations. Given a scanned image of the target random medium, this method starts from an initial configuration satisfying the volume fraction, and for the simulated image it successively performs random exchanges of pixels with different colors to minimize certain “energy” that measures the difference in correlation function, two-point cluster function [9] or n -point correlation function [10] etc. between the reference image and the simulated image. If the energy decreases after the exchange, the new configuration is considered superior to the old one, and the exchange is accepted. If the energy increases after the exchange, the new configuration is considered possible to be a transitional state from “local optimum” to “global optimum”, and hence the exchange is accepted with a probability, which depends on the energy of the old and the new configurations and the annealing temperature [1]. Recently, several other stochastic optimization approaches were developed to overcome the low efficiency of the simulated annealing method, including genetic algorithm, Tabu-list and hybrid optimization methods [3,11]. The stochastic optimization method is perhaps the most flexible method for reconstructing random media samples, and it allows a wide range of statistical characteristics to be incorporated in sample generation. Its disadvantage is the expensive computational burden when large samples (either in size or in number) are required.

In the maximum entropy method [10,12,13], random media are modeled as Markov random fields. The joint probability distribution of Markov random fields is the Gibbs distribution [14], which is exactly the probability distribution that maximizes the entropy under expectation-type confinements (e.g. μ , σ^2 , $R_f(\tau)$, etc) [15,16]. The explicit formation of the Gibbs distribution cannot be obtained because it is an infinite dimensional function. Thus, Markov chain Monte Carlo (MCMC) methods [17] are employed to sample from the Gibbs distribution, for which the Metropolis–Hastings algorithm [18,19] (a random walk MCMC method) has been a popular choice. Similar to the stochastic optimization method, which can be viewed as a special type of the Metropolis–Hastings algorithm [19,20], a large number of random walk steps are often required to achieve the equilibrium distribution status of the Markov chain. For practical use, the maximum entropy method is criticized to be even slower than the stochastic optimization method, and not suitable for large size problems [3].

The nonlinear transformation of Gaussian fields has been extensively used in modeling multivariate distributions [21,22]. The marginal distribution of the non-Gaussian field is met exactly,

and the covariance of the underlying Gaussian field is computed numerically to satisfy the two point covariance requirement of the non-Gaussian field. This approach has been employed to model two-phase random media [2,23,24]. However, the relationship between the covariance of the non-Gaussian field and that of the Gaussian field is ignored in [23,24], while using an iterative algorithm the covariance function of the underlying Gaussian field is calculated in [2]. The most costly part of the nonlinear transformation approach is to determine the nonnegative definite covariance function (nonnegative definite covariance matrix in the discrete case) of the underlying Gaussian field. In most of the literature [2] and [25–28], the Gaussian field is constructed from an initial power spectral density (PSD) structure and an iterative algorithm is adopted to repeatedly update the PSD of the Gaussian field in order to make the PSD of the non-Gaussian field meet the target, and this can be a very slow process for practical problems. Another limitation of this method is that the marginal distribution and the covariance of the non-Gaussian field need to satisfy a compatibility relation in advance [29].

In this paper, the relationship between the correlation of the binary field and that of the Gaussian field is derived explicitly to avoid the costly iteration procedure commonly employed in existing nonlinear transformation approaches. The compatibility relation between the marginal distribution and the autocorrelation of binary valued fields are also rigorously investigated, and proved to be not a critical restriction. These new developments significantly improve the efficiency of sample generation, allowing thousands of large samples to be generated within a few minutes. The main limitation of the method is that it does not utilize other statistical characteristics (e.g. n -point correlation and lineal-path function). However, numerical examples demonstrate that the new method is suitable for a variety of types of two-phase random media, as two-point correlation contains considerable information on random morphology.

2.2. Preliminary knowledge: spectral decomposition of stationary random fields

The Wiener–Khinchin theorem [30,31] states that the PSD $f(\mathbf{X})$ of a stationary second-order random field $a(\mathbf{x}, \omega)$ is the Fourier transform of the corresponding autocorrelation function $R(\tau)$. If $a(\mathbf{x}, \omega)$ is a periodical stochastic process [32,33] with a period of $2N$, i.e. $a(x_1, \dots, x_n, \omega) = a(x_1 + 2N_1, \dots, x_n + 2N_n, \omega)$, the discrete version of the Wiener–Khinchin theorem can be written as [34,35]:

$$f(X_1, \dots, X_n) = \sum_{\tau_1=-N_1+1}^{N_1} \dots \sum_{\tau_n=-N_n+1}^{N_n} R(\tau_1, \dots, \tau_n) e^{-\sum_{j=1}^n \frac{2\pi i X_j \tau_j}{N_j}},$$

$$X_j = [-N_j + 1, N_j] \tag{3}$$

$$R(\tau_1, \dots, \tau_n) = \frac{1}{\prod_j (2N_j)} \sum_{X_1=-N_1+1}^{N_1} \dots \sum_{X_n=-N_n+1}^{N_n} f(X_1, \dots, X_n) e^{\sum_{j=1}^n \frac{2\pi i X_j \tau_j}{N_j}},$$

$$\tau_j = [-N_j + 1, N_j] \tag{4}$$

where i is the imaginary unit, N_j are positive integers, the integer coordinates τ_1, \dots, τ_n denote the space domain, the integer coordinates X_1, \dots, X_n denote the frequency domain, and $f(X_1, \dots, X_n)$ is real and nonnegative valued due to the nonnegative definite property of $R(\tau_1, \dots, \tau_n)$.

Then, $a(\mathbf{x}, \omega)$ can be represented by an orthogonal increment process:

$$a(\mathbf{x}_1, \dots, \mathbf{x}_n, \omega) = E(a(\mathbf{x}_1, \dots, \mathbf{x}_n, \omega)) + \frac{1}{\prod_{j=1}^n (2N_j)} \sum_{X_1=-N_1+1}^{N_1} \dots \sum_{X_n=-N_n+1}^{N_n} \xi(\mathbf{x}_1, \dots, \mathbf{x}_n, \omega) e^{j=1} \sum_{N_j}^{X_j} X_j, \quad (5)$$

$$x_j = [-N_j + 1, N_j]$$

where $\xi(\mathbf{x}_1, \dots, \mathbf{x}_n, \omega)$ are uncorrelated, complex valued random variables satisfying

$$E(\xi(X_{z1}, \dots, X_{zn}, \omega)) = 0 \quad \forall X_{zj} \in \mathbb{Z}[-N_j + 1, N_j] \quad (6)$$

and

$$E(\xi(X_{z1}, \dots, X_{zn}, \omega) \overline{\xi(X_{\beta 1}, \dots, X_{\beta n}, \omega)}) = \begin{cases} \prod_{j=1}^n (2N_j) f(X_{z1}, \dots, X_{zn}) \sigma^2 & \text{if } X_{zj} = X_{\beta j}, \forall j \\ 0 & \text{else} \end{cases} \quad \forall X_{zj}, X_{\beta j} \in \mathbb{Z}[-N_j + 1, N_j]. \quad (7)$$

Especially, if $a(\mathbf{x}_1, \dots, \mathbf{x}_n, \omega)$ is a Gaussian random field, then $\xi(\mathbf{x}_1, \dots, \mathbf{x}_n, \omega)$ are all independent complex Gaussian random variables.

The Wiener–Khinchin theorem, which is a second order statistical decomposition method, plays an important role in the analysis of stationary Gaussian fields as Gaussian fields are completely determined by their first two statistical moments. However, for non-Gaussian random fields, it is difficult to directly generate samples because the uncorrelated random variables $\xi(\mathbf{x}_1, \dots, \mathbf{x}_n, \omega)$ are not independent and their joint probability distribution is unknown a priori.

3. Nonlinear transformation of Gaussian fields

Let $G(\mathbf{x}, \omega)$ be a stationary Gaussian field with zero mean and unit variance, and let $R_G(\boldsymbol{\tau})$ denote its autocorrelation function. The Gaussian field $G(\mathbf{x}, \omega)$ is uniquely determined by $R_G(\boldsymbol{\tau})$. The marginal distribution of $G(\mathbf{x}, \omega)$ can be expressed as

$$F_G(y) = \frac{1}{2} \left[1 + \operatorname{erf} \left(\frac{y}{\sqrt{2}} \right) \right] \quad (8)$$

where $\operatorname{erf}(\cdot)$ denotes the error function.

To reconstruct the two-phase random medium defined by $I(\mathbf{x}, \omega)$ in Eq. (1), we aim to find a transformation of $G(\mathbf{x}, \omega)$ such that $R_G(\boldsymbol{\tau})$ can be explicitly specified to give the transformed Gaussian field the same mean, variance, covariance (or autocorrelation) and marginal distribution as $I(\mathbf{x}, \omega)$. Let p_0 denote the volume fraction of the black phase. It is then trivial to obtain the mean and variance of $I(\mathbf{x}, \omega)$ as

$$\mu = 1 - p_0, \quad (9)$$

$$\sigma^2 = p_0(1 - p_0). \quad (10)$$

Define a transformation function $T(y)$ as

$$T(y) = \begin{cases} 0 & \text{if } y \leq F_G^{-1}(p_0) \\ 1 & \text{if } y > F_G^{-1}(p_0) \end{cases} \quad (11)$$

where $F_G^{-1}(p_0)$ is the separation point at which the distribution $F_G(y)$ takes the value of p_0 . Let

$$I^*(\mathbf{x}, \omega) = T(G(\mathbf{x}, \omega)). \quad (12)$$

It is easy to verify that the transformed random field $I^*(\mathbf{x}, \omega)$ is stationary and has the same marginal distribution, mean and variance as $I(\mathbf{x}, \omega)$. The next step is to determine $R_G(\boldsymbol{\tau})$ so that $I^*(\mathbf{x}, \omega)$ follows the same autocorrelation $R_I(\boldsymbol{\tau})$. Once $R_G(\boldsymbol{\tau})$ is determined, it is straightforward to generate samples of $G(\mathbf{x}, \omega)$ following the Wiener–Khinchin theorem (3)–(7), which can be further transformed to produce samples of $I(\mathbf{x}, \omega)$.

3.1. The relationship between autocorrelations $R_G(\boldsymbol{\tau})$ and $R_I(\boldsymbol{\tau})$

For any two points \mathbf{x}_1 and $\mathbf{x}_2 = \mathbf{x}_1 + \boldsymbol{\tau}$ in the medium, the autocorrelation function of the transformed two-phase random medium $I^*(\mathbf{x}, \omega)$ can be computed by substituting Eq. (12) into Eq. (2), i.e.

$$R_I^*(\boldsymbol{\tau}) = \frac{E[(T(G(\mathbf{x}_1, \omega)) - \mu)(T(G(\mathbf{x}_2, \omega)) - \mu)]}{\sigma^2} = \int_{-\infty}^{+\infty} \int_{-\infty}^{+\infty} \frac{(T(y_1) - \mu)(T(y_2) - \mu)}{\sigma^2} f_{g2}(y_1, y_2, R_G(\boldsymbol{\tau})) dy_1 dy_2 \quad (13)$$

where

$$f_{g2}(y_1, y_2, R_G(\boldsymbol{\tau})) = \frac{1}{2\pi\sqrt{1 - R_G(\boldsymbol{\tau})^2}} \times \exp \left(\frac{-1}{2(1 - R_G(\boldsymbol{\tau})^2)} (y_1^2 + y_2^2 - 2R_G(\boldsymbol{\tau})y_1y_2) \right) \quad (14)$$

is the joint probability density function (PDF) of a standard bivariate Gaussian distribution with zero mean, unit variance and autocorrelation $R_G(\boldsymbol{\tau})$.

Following Eq. (11), the integrand $\frac{(T(y_1) - \mu)(T(y_2) - \mu)}{\sigma^2}$ in Eq. (13) can be computed as

$$\frac{(T(y_1) - \mu)(T(y_2) - \mu)}{\sigma^2} = \begin{cases} (1 - p_0)/p_0 & \text{if } y_1 \in (-\infty, F_G^{-1}(p_0)], y_2 \in (-\infty, F_G^{-1}(p_0)) \\ -1 & \text{if } y_1 \in (-\infty, F_G^{-1}(p_0)], y_2 \in (F_G^{-1}(p_0), \infty) \\ -1 & \text{if } y_1 \in (F_G^{-1}(p_0), \infty), y_2 \in (-\infty, F_G^{-1}(p_0)] \\ p_0/(1 - p_0) & \text{if } y_1 \in (F_G^{-1}(p_0), \infty), y_2 \in (F_G^{-1}(p_0), \infty) \end{cases} \quad (15)$$

Substituting Eqs. (15) into (13) yields

$$R_I^*(\boldsymbol{\tau}) = -1 + \frac{1}{p_0} \int_{-\infty}^{F_G^{-1}(p_0)} \int_{-\infty}^{F_G^{-1}(p_0)} f_{g2}(y_1, y_2, R_G(\boldsymbol{\tau})) dy_1 dy_2 + \frac{1}{1 - p_0} \int_{F_G^{-1}(p_0)}^{+\infty} \int_{F_G^{-1}(p_0)}^{+\infty} f_{g2}(y_1, y_2, R_G(\boldsymbol{\tau})) dy_1 dy_2. \quad (16)$$

Due to the symmetry of $f_{g2}(y_1, y_2, R_G(\boldsymbol{\tau}))$ (14), i.e. $f_{g2}(y_1, y_2, R_G(\boldsymbol{\tau})) = f_{g2}(-y_1, -y_2, R_G(\boldsymbol{\tau}))$, the autocorrelation $R_I^*(\boldsymbol{\tau})$ can be further simplified into

$$R_I^*(\boldsymbol{\tau}) = -1 + \frac{1}{p_0} \int_{-\infty}^{F_G^{-1}(p_0)} \int_{-\infty}^{F_G^{-1}(p_0)} f_{g2}(y_1, y_2, R_G(\boldsymbol{\tau})) dy_1 dy_2 + \frac{1}{1 - p_0} \int_{-\infty}^{-F_G^{-1}(p_0)} \int_{-\infty}^{-F_G^{-1}(p_0)} f_{g2}(y_1, y_2, R_G(\boldsymbol{\tau})) dy_1 dy_2 = -1 + \frac{1}{p_0} F_{g2}(F_G^{-1}(p_0), F_G^{-1}(p_0), R_G(\boldsymbol{\tau})) + \frac{1}{1 - p_0} F_{g2}(-F_G^{-1}(p_0), -F_G^{-1}(p_0), R_G(\boldsymbol{\tau})) \quad (17)$$

where

$$F_{g2}(y_1, y_2, R_G(\boldsymbol{\tau})) = \int_{-\infty}^{y_1} \int_{-\infty}^{y_2} f_{g2}(z_1, z_2, R_G(\boldsymbol{\tau})) dz_1 dz_2 \quad (18)$$

is the cumulative distribution function corresponding to the PDF $f_{g2}(y_1, y_2, R_G(\boldsymbol{\tau}))$.

In Eq. (17), the relationship between $R_I^*(\boldsymbol{\tau})$ and $R_G(\boldsymbol{\tau})$ depends on the volume fraction p_0 . Due to the symmetry of the PDF $f_{g2}(y_1, y_2, R_G(\boldsymbol{\tau}))$, it is straightforward to prove that

$$R_i^*(\tau, p_0) = R_i^*(\tau, 1 - p_0). \tag{19}$$

For a fixed volume fraction p_0 , Eq. (17) explicitly expresses $R_i^*(\tau)$, the autocorrelation of the transformed two-phase random media, as a nonlinear function of $R_G(\tau)$, the autocorrelation of the underlying Gaussian random field. Given the value of $R_i^*(\tau)$, the corresponding $R_G(\tau)$ can be solved, at least in principle, through an iterative solver. It is proved in the following section that $R_i^*(\tau)$ is monotonic with respect to $R_G(\tau)$. Hence, the solution of $R_G(\tau)$ can be significantly simplified through precomputation.

3.2. Compatibility relation between marginal distribution and autocorrelation

Following Eq. (17), the derivative of $R_i^*(\tau)$ with respect to $R_G(\tau)$ can be expressed as

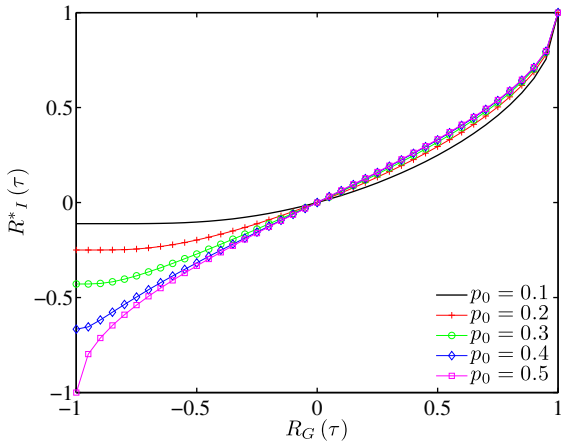


Fig. 1. Precomputed $R_i^*(\tau) - R_G(\tau)$ curves.

$$\begin{aligned} \frac{dR_i^*(\tau)}{dR_G(\tau)} &= \frac{1}{p_0} \int_{-\infty}^{F_G^{-1}(p_0)} \int_{-\infty}^{F_G^{-1}(p_0)} \frac{df_{g2}(y_1, y_2, R_G(\tau))}{dR_G(\tau)} dy_1 dy_2 \\ &+ \frac{1}{1-p_0} \int_{-\infty}^{-F_G^{-1}(p_0)} \int_{-\infty}^{-F_G^{-1}(p_0)} \frac{df_{g2}(y_1, y_2, R_G(\tau))}{dR_G(\tau)} dy_1 dy_2 \end{aligned} \tag{20}$$

where

$$\begin{aligned} \frac{df_{g2}(y_1, y_2, R_G(\tau))}{dR_G(\tau)} &= \frac{-R_G(\tau)(y_1^2 + y_2^2) + (R_G(\tau)^2 + 1)y_1 y_2 + R_G(\tau)(1 - R_G(\tau)^2)}{(1 - R_G(\tau)^2)^2} \\ &\times f_{g2}(y_1, y_2, R_G(\tau)). \end{aligned} \tag{21}$$

It can be computed that

$$\int_{-\infty}^z \int_{-\infty}^z \frac{df_{g2}(y_1, y_2, R_G(\tau))}{dR_G(\tau)} dy_1 dy_2 = \frac{\exp\left(-\frac{z^2}{1+R_G(\tau)}\right)}{2\pi\sqrt{1-R_G(\tau)^2}} \quad \forall z \in [-\infty, +\infty]. \tag{22}$$

Thus, the derivative (20) can be simplified as

$$\frac{dR_i^*(\tau)}{dR_G(\tau)} = \left(\frac{1}{p_0} + \frac{1}{1-p_0}\right) \frac{\exp\left(-\frac{(F_G^{-1}(p_0))^2}{1+R_G(\tau)}\right)}{2\pi\sqrt{1-R_G(\tau)^2}} \geq 0. \tag{23}$$

Eq. (23) implies that $R_i^*(\tau)$ is monotonically increasing with respect to $R_G(\tau)$. Hence, the range of $R_i^*(\tau)$ can be determined as:

$$\begin{aligned} \max(R_i^*(\tau)) &= \lim_{R_G(\tau) \rightarrow 1} \int_{-\infty}^{+\infty} \int_{-\infty}^{+\infty} \frac{(T(y_1) - \mu)(T(y_2) - \mu)}{\sigma^2} \\ &\times f_{g2}(y_1, y_2, R_G(\tau)) dy_1 dy_2 = 1, \end{aligned} \tag{24}$$

$$\begin{aligned} \min(R_i^*(\tau)) &= \lim_{R_G(\tau) \rightarrow -1} \int_{-\infty}^{+\infty} \int_{-\infty}^{+\infty} \frac{(T(y_1) - \mu)(T(y_2) - \mu)}{\sigma^2} \\ &\times f_{g2}(y_1, y_2, R_G(\tau)) dy_1 dy_2 = -\frac{\min(p_0, 1-p_0)}{\max(p_0, 1-p_0)}. \end{aligned} \tag{25}$$

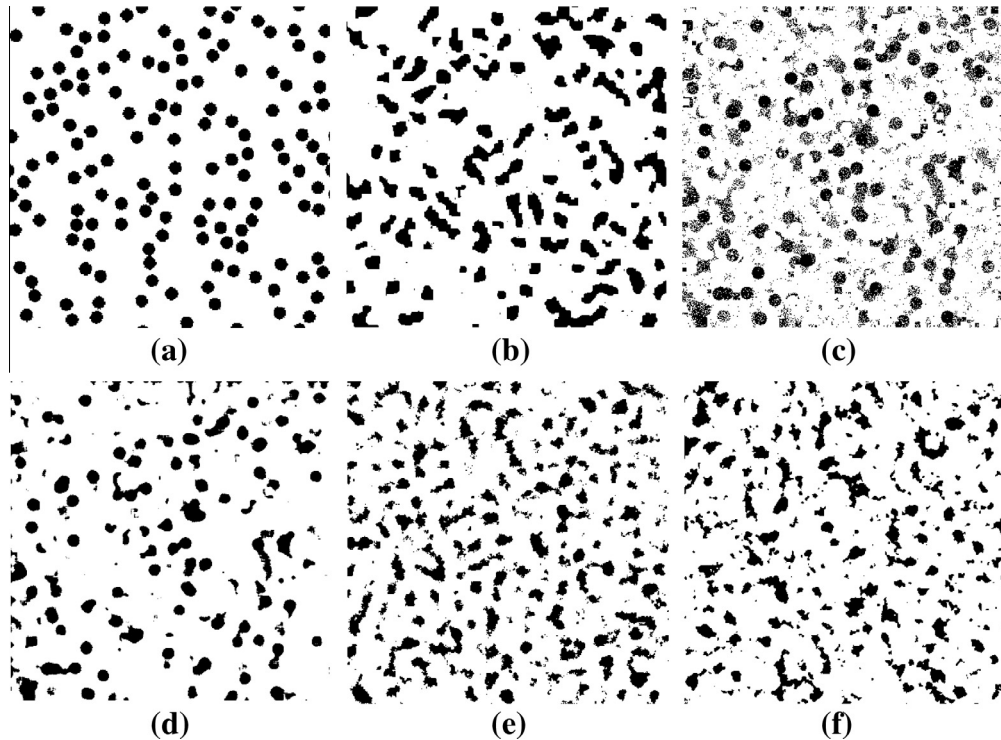


Fig. 2. Comparison 1, image size 400×400 pixels. (a) The reference random media sample from [1]; (b) the random media sample reconstructed by the simulated annealing method in [1]; (c) a random media sample directly generated by our simulated annealing code; (d) the final sample after median filtering of (c); (e) a random media sample reconstructed by the iterative nonlinear transformation method; (f) a random media sample reconstructed by the proposed method.

The above equations set the upper and lower limits of the autocorrelation $R_I^*(\tau)$, which depend on the volume fraction p_0 . They form a necessary condition for reconstructing the target random medium through the proposed nonlinear transformation of the Gaussian field. That is, a two-phase random medium with volume fraction p_0 and autocorrelation $R_I(\tau)$ can be reconstructed only if $R_I(\tau) \in \left[-\frac{\min(p_0, 1-p_0)}{\max(p_0, 1-p_0)}, 1\right]$. Note that, for practical random media with irregular structures, the autocorrelation functions are almost always above zero [9]. Hence, conditions (24)–(25) do not form a serious restriction for the proposed method.

3.3. Computational issues

Given the autocorrelation $R_I(\tau)$ of the target two-phase random medium, to solve the autocorrelation $R_G(\tau)$ of the underlying Gaussian random field from the nonlinear Eq. (17) is potentially time consuming, if an iterative solver has to be adopted. Noting that the relationship between $R_I^*(\tau)$ and $R_G(\tau)$ is monotonic, one can precompute the function curve between $R_I^*(\tau)$ and $R_G(\tau)$ to save the costly procedure of solving nonlinear equations. An example is shown in Fig. 1, where according to Eq. (17), the $R_G(\tau) \rightarrow R_I^*(\tau)$ curves are computed for five volume fractions $p_0 = 0.1$,

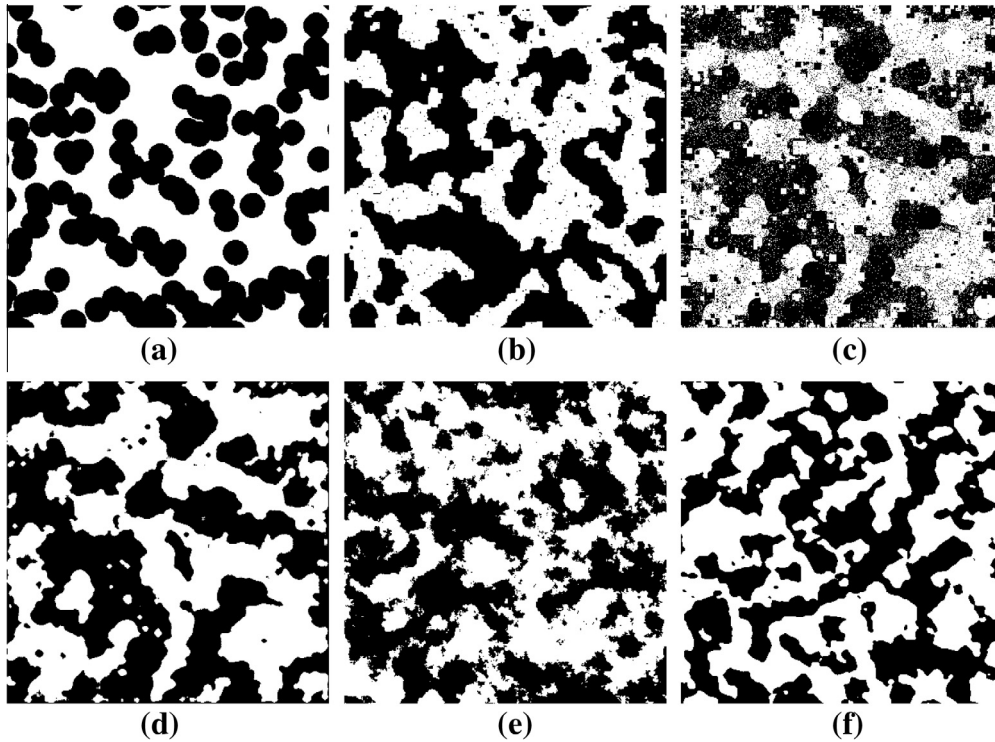


Fig. 3. Comparison 2, image size 400×400 pixels. (a) The reference random media sample from [1]; (b) the random media sample reconstructed by the simulated annealing method in [1]; (c) a random media sample directly generated by our simulated annealing code; (d) the final sample after median filtering of (c); (e) a random media sample reconstructed by the iterative nonlinear transformation method; (f) a random media sample reconstructed by the proposed method.

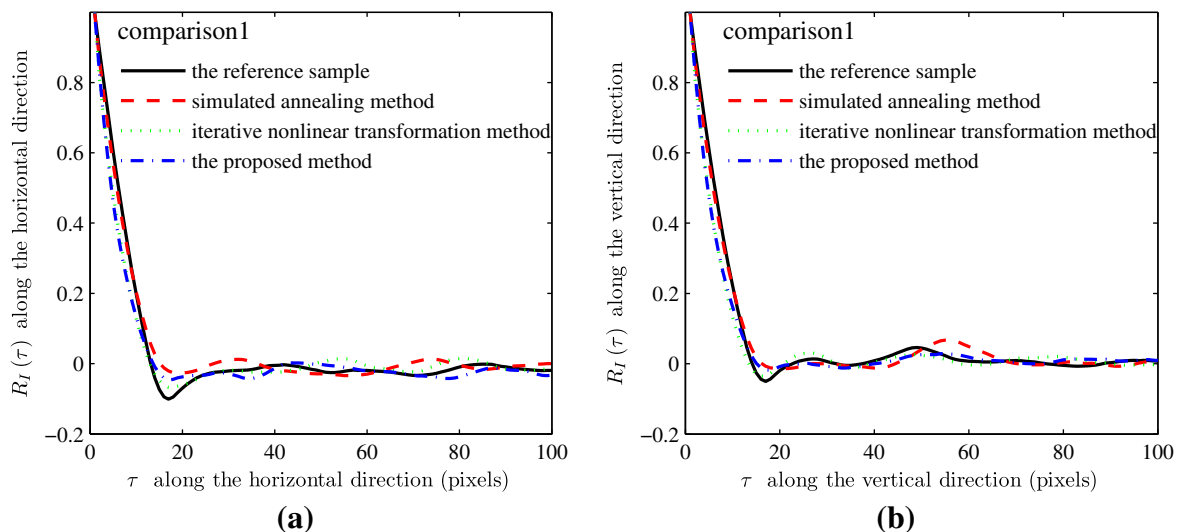


Fig. 4. Autocorrelation functions of the samples in the first comparison. (a) The autocorrelation along the horizontal direction; (b) the autocorrelation along the vertical direction.

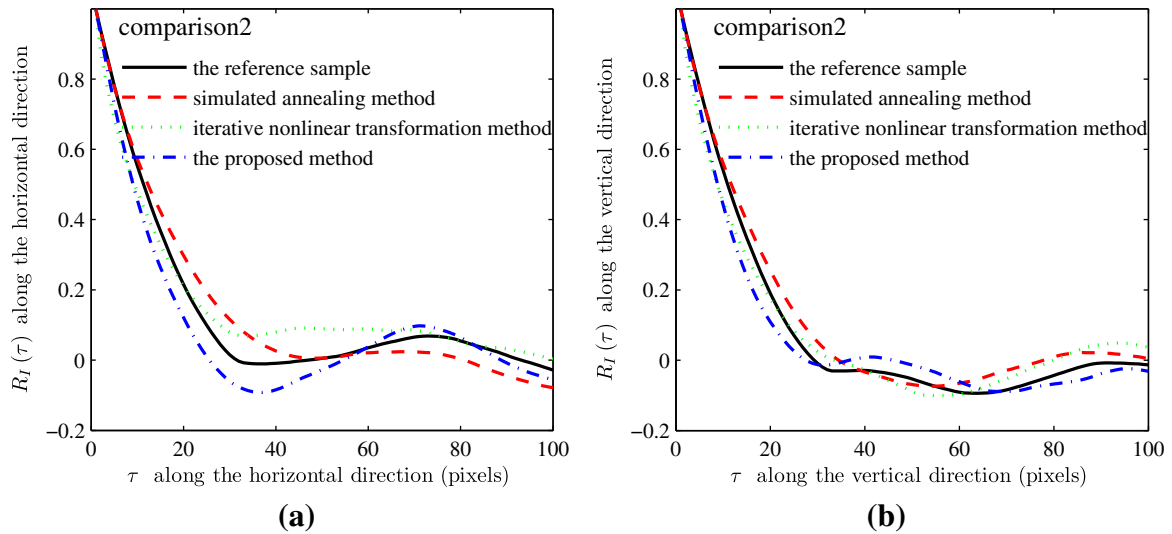


Fig. 5. Autocorrelation functions of the samples in the second comparison. (a) The autocorrelation along the horizontal direction; (b) the autocorrelation along the vertical direction.

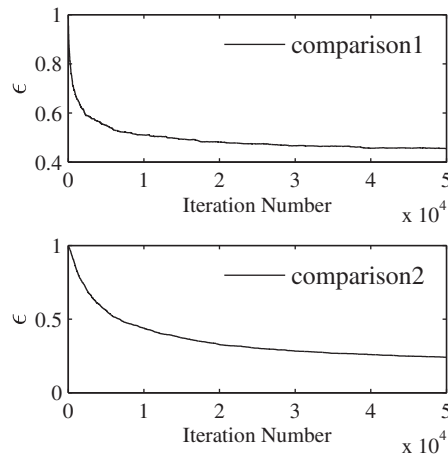


Fig. 6. Convergence curves of the simulated annealing method.

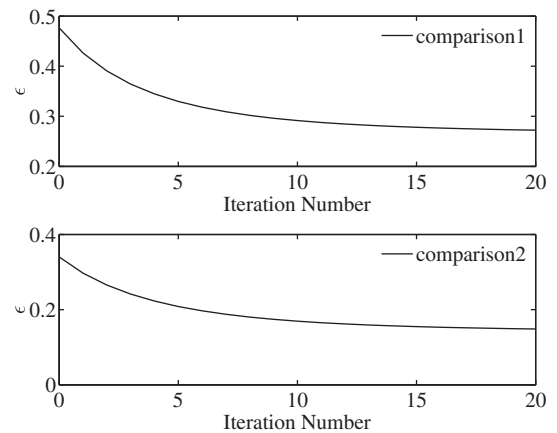


Fig. 7. Convergence curves of the iterative nonlinear transformation method.

0.2, . . . , 0.5. Due to the symmetry relation in Eq. (19), the $R_G(\tau) \rightarrow R_I^*(\tau)$ curves for $p_0 = 0.6, 0.7, \dots, 0.9$ are symmetric. Thus, given the volume fraction p_0 and the target autocorrelation $R_I(\tau)$, the corresponding autocorrelation $R_G(\tau)$ for the underlying Gaussian field can be readily obtained from these precomputed curves through interpolation. Doing so avoids the expensive solution procedure of the nonlinear $R_G(\tau) \rightarrow R_I^*(\tau)$ equation, and can significantly accelerate sample reconstruction.

In the discrete case, function $R_G(\tau)$ can be expressed as a covariance matrix with unit diagonal entries and the absolute values of off diagonal entries less than one. Due to numerical approximation, the resulting matrix $R_G(\tau)$ may contain a few small negative eigenvalues, violating the nonnegative definite requirement for a covariance matrix. Hence, a “nearest correlation matrix” [36–38] should be constructed, which is a common practice for multivariate analysis. To do this, we compute the PSD of $R_G(\tau)$ (see Eq. (3)) and set the negative PSD entries to zero, after which the truncated PSD is transformed back following Eq. (4) to form a nonnegative definite covariance matrix, ready for use on the Gaussian field.

4. Summary of the algorithm

The algorithm framework of the proposed sample generation method is summarized below.

-
- Given a reference sample $I(\mathbf{x}, \omega)$, count the volume fraction p_0 and estimate its autocorrelation function $R_I(\tau)$ through FFT (fast Fourier transform) of the sample spectrum. This is a standard practice of random signal processing, for which detailed description can be found in [39,40] and [41]. Note: the random medium is assumed with a $2N$ periodic boundary as shown in Eqs. (3) and (4). The period $2N$ is larger than the size of the random medium and selected as a power of 2 to enhance the efficiency of FFT, thus padding with 0 is required [39,40].
 - For the measured volume fraction p_0 , plot the $R_I^*(\tau) - R_G(\tau)$ curve according to Eq. (17). The result is monotonic and example curves are shown in Fig. 1.
 - Construct the covariance matrix of the underlying Gaussian field, by registering the $R_I^*(\tau) - R_G(\tau)$ curve with the measured autocorrelation $R_I(\tau)$ of the target two-phase random medium.
 - Generate Gaussian field samples $G(\mathbf{x}, \omega)$, by using the spectral decomposition method (3)–(7). This step is performed with FFT.
 - Generate samples of $I(\mathbf{x}, \omega)$ through the nonlinear transformation (11).
-

Table 1
Computational cost of sample reconstruction.

Example no.	Simulated annealing	Iterative nonlinear transformation	The proposed method
Comparison 1	635 s	10070 s, 20 iterations	4 s, no iteration
Comparison 2	696 s	9694 s, 20 iterations	4 s, no iteration

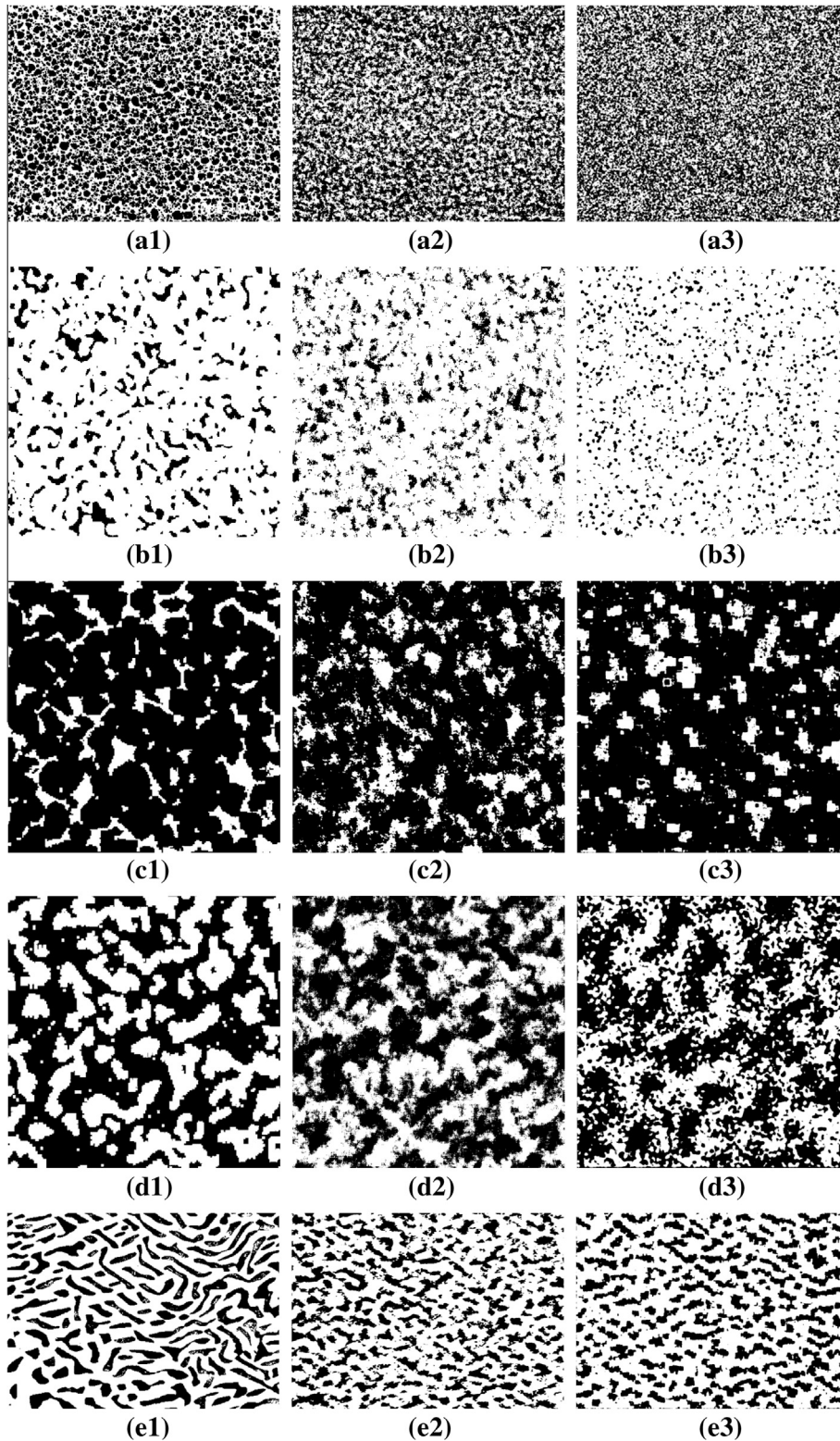


Fig. 8. 2D random media reconstruction. (a1–e1) The reference random media samples; (a2–e2) the random media samples reconstructed by the proposed method; (a3–e3) the random media samples reconstructed by the simulated annealing method.

The main computational cost of the proposed algorithm is the FFT operation involved in step 4, whose computational complexity is $\log L$ proportional to the reconstructed sample size L . This high computational efficiency allows large sample sets (in terms of both sample size and sample number) to be reconstructed on a commodity computer with moderate cost. The efficiency and accuracy of the proposed method are demonstrated by a number of examples in the next section with comparisons to other state-of-the-art methods.

A free MATLAB® code of the proposed method is available upon request.

5. Examples

A number of examples are presented in this section to demonstrate the performance of the proposed method. First, the new method is compared with other state-of-the-art methods in the literature, including the simulated annealing method [1] and the iterative nonlinear transformation method [26,28]. The random set method [4–6] and the maximum entropy method [10,12,13] are not chosen for comparison, because the former is limited to a few special geometries, and the latter has high computational

and implementation complexity. After the comparison, the new method is applied to a wide range of different random media to demonstrate its accuracy and applicability. Finally, large-scale 3D cases are considered, and the new method is used to reconstruct 3D samples for nuclear graphite Gilsocarbon measured from three-dimensional X-ray scanning.

All examples are simulated on a PC with an Intel Core i7 3.40 GHz processor and 16 GB memory.

5.1. Comparison

To help examine the performance of the proposed method, we have also implemented the simulated annealing method [1] and the iterative nonlinear transformation method [26,28]. For comparison, we took two random media samples from [1], and reconstructed the associated samples using three different methods. Shown in Fig. 2(a) and (b) are a random media example and a reconstructed sample taken from [1]. Fig. 2(c) and (d) is a sample reconstructed using our own implementation of the simulated annealing method and for fair comparison, we adopted the same algorithmic parameters as [1]. As the pixel exchanges are operated on disks with a diameter of 17 pixels, the direct reconstruction

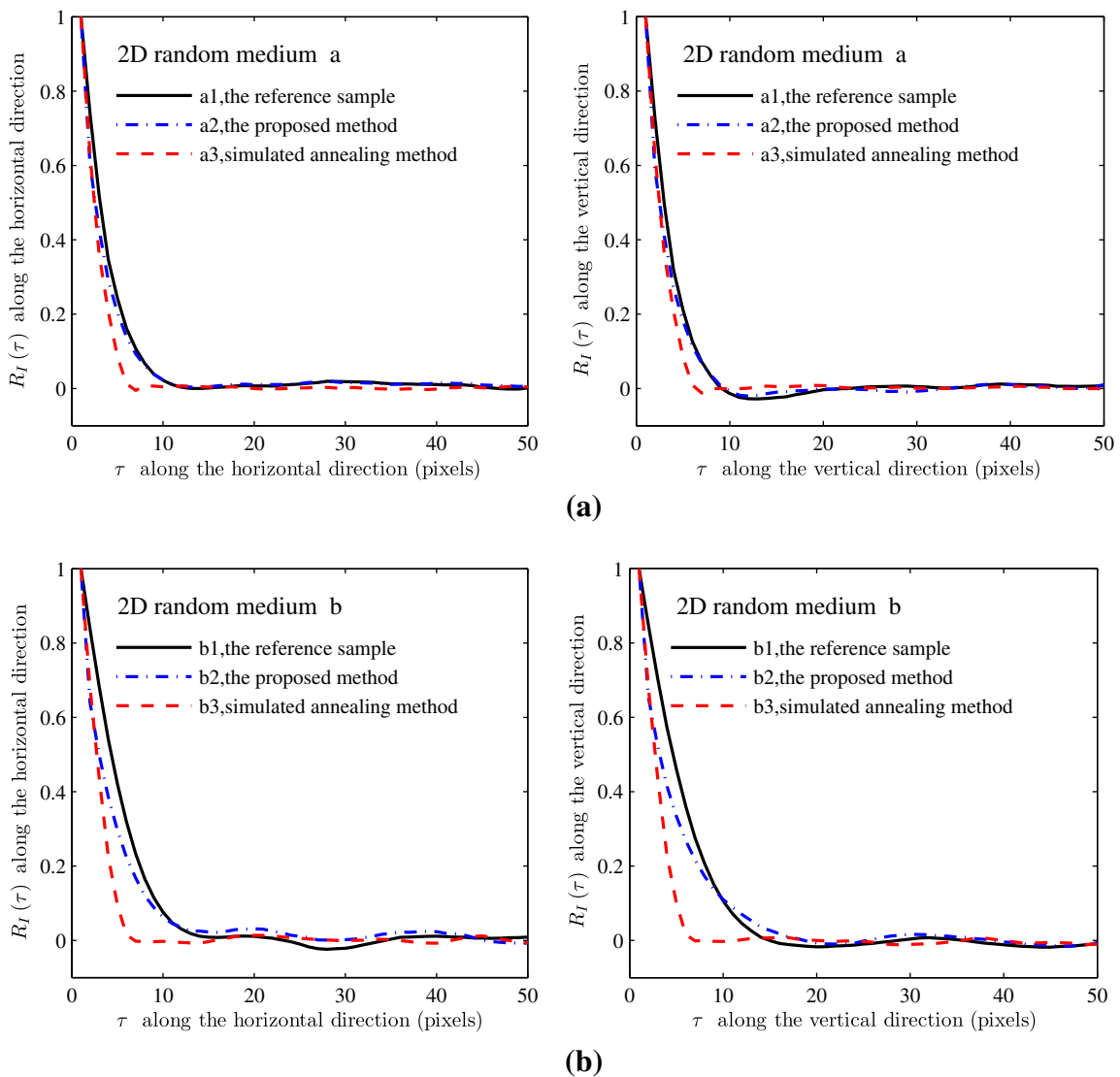


Fig. 9. Autocorrelation functions of the 2D random media samples in Fig. 8. Left: the autocorrelations along the horizontal direction; right: the autocorrelations along the vertical direction.

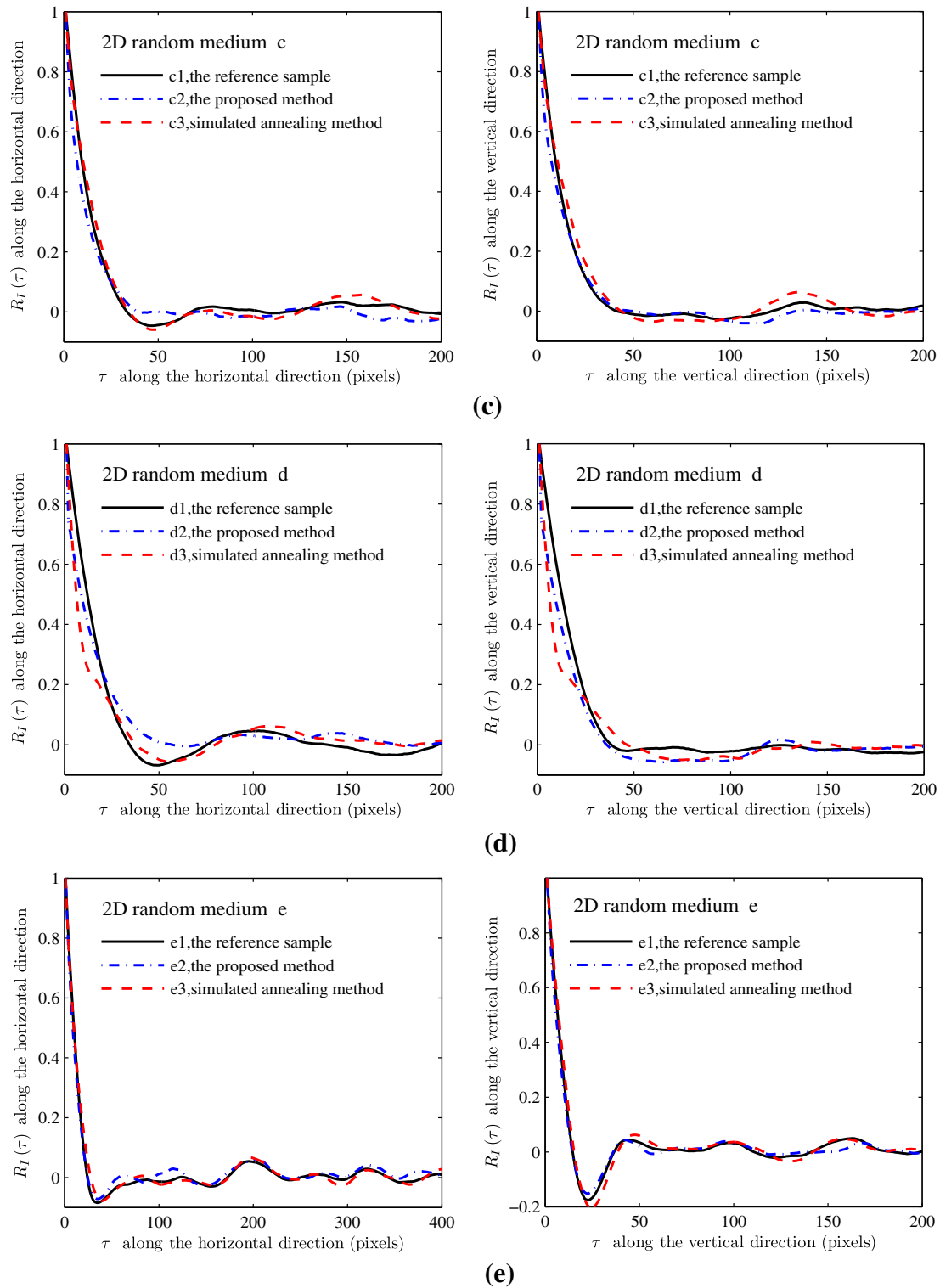


Fig. 9. (continued)

(Fig. 2(c)) inevitably contains “salt and pepper” noises [10], which are removed by 2D median filtering to produce the reconstructed sample (Fig. 2(d)). Fig. 2(e)–(f) are two samples reconstructed using the iterative nonlinear transformation method and our new method, respectively. For a random media sample with different morphology, a similar comparison is presented in Fig. 3.

Comparing the simulated annealing results in Figs. 2(b) and (d) and 3(b) and (d), it can be seen that our implementation produces

similar results as the original work in [1]. To further examine the accuracy of the different methods, the autocorrelation functions calculated from Figs. 2(d)–(f) and 3(d)–(f) are plotted in Figs. 4 and 5 respectively, where Figs. 4(a) and 5(a) show the autocorrelations along the horizontal direction, and Figs. 4(b) and 5(b) show the autocorrelations along the vertical direction. It can be seen that all three methods achieve similar levels of accuracy in the sense of autocorrelation.

Both the simulated annealing method and the iterative nonlinear transformation method require repeatedly comparing the auto-correlations of the target random field and the reconstructed random field. To retain the nonnegative definite property of the autocorrelation, the comparison is usually performed through comparing the PSD $f(X)$ in Eq. (3). Let $f_t(X)$ and $f_c(X)$ denote respectively the PSD of the target random field and the reconstructed random field, and define the error function ε as:

$$\varepsilon = \frac{\sqrt{\sum (f_c(X) - f_t(X))^2}}{\sqrt{\sum f_t(X)^2}}, \tag{26}$$

where the sum operation is performed over all discretized frequencies. In the simulated annealing method, the function ε is taken as

the energy function and a pixel exchange is accepted if ε decreases; and vice versa. In the iterative nonlinear transformation method, the function ε is used as the stopping criterion [28], and the iteration is terminated if ε is reduced below a given threshold. The main computational cost in the simulated annealing method and the iterative nonlinear transformation method arise from the repeated computation of $f_c(X)$. For the simulated annealing method, $f_c(X)$ is computed after each pixel exchange step, through FFT of the reconstructed image [39]. For the iterative nonlinear transformation method, $f_c(X)$ is computed in each iteration step as the FFT of the autocorrelation function of the reconstructed sample, which is calculated through a probability integral of the underlying Gaussian field [28].

Shown in Fig. 6 are the convergence curves for the simulated annealing method, and shown in Fig. 7 are the convergence curves

Table 2
Performance data for 2D random media reconstruction.

Random media no.	a	b	c	d	e
Image size (pixel × pixel)	564 × 710	436 × 438	685 × 684	682 × 682	657 × 909
CPU time cost of the proposed method (s)	0.023	0.010	0.029	0.025	0.035
CPU time cost of simulated annealing (s)	3474	1826	2951	5022	3926
p_0	0.5226	0.1442	0.8085	0.5451	0.3484
Measured bounds of $R_l(\tau)$	[-0.0416,1]	[-0.0344,1]	[-0.0535,1]	[-0.0796,1]	[-0.1794,1]
Compatibility bounds of $R_l(\tau)$	[-0.9136,1]	[-0.1686,1]	[-0.2369,1]	[-0.8345,1]	[-0.5348,1]

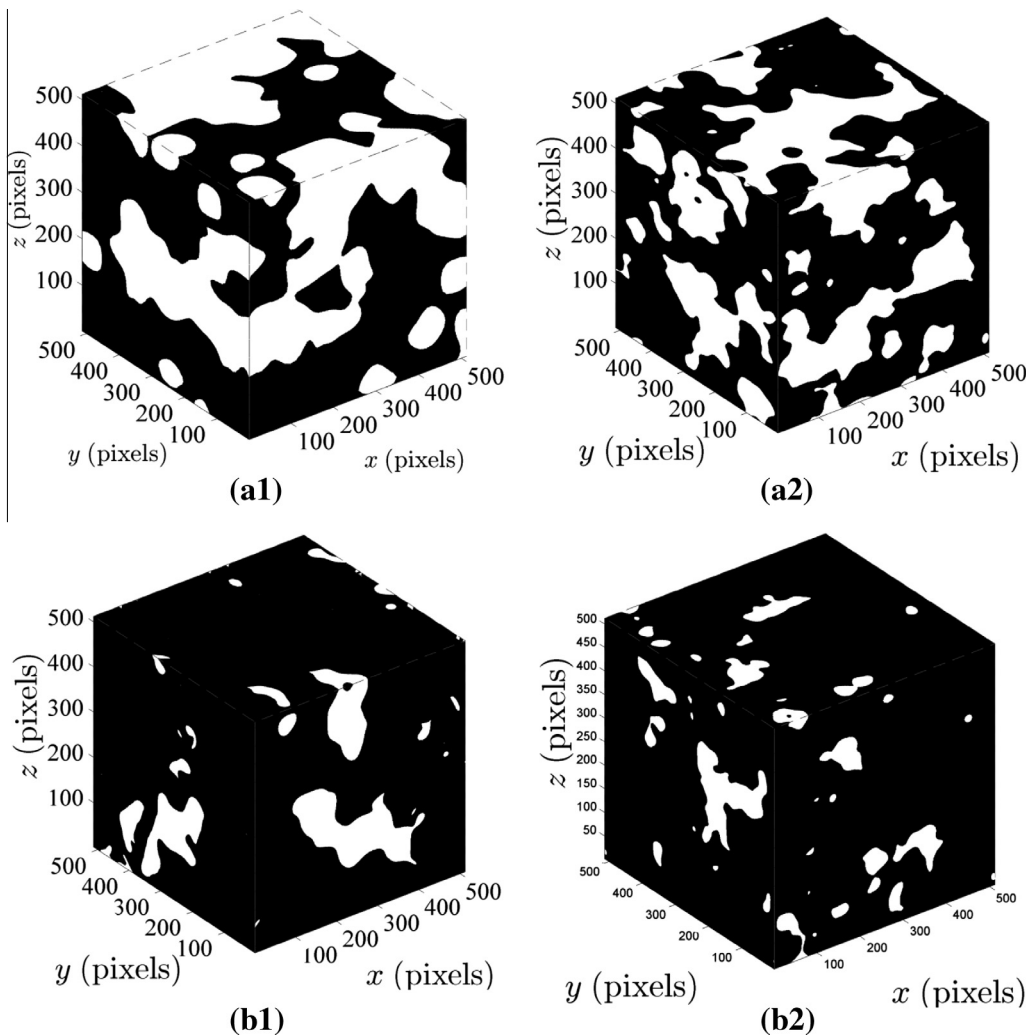


Fig. 10. 3D random media reconstruction. (a1–d1) The reference random media samples; (a2–d2) the random media samples reconstructed by the proposed method.

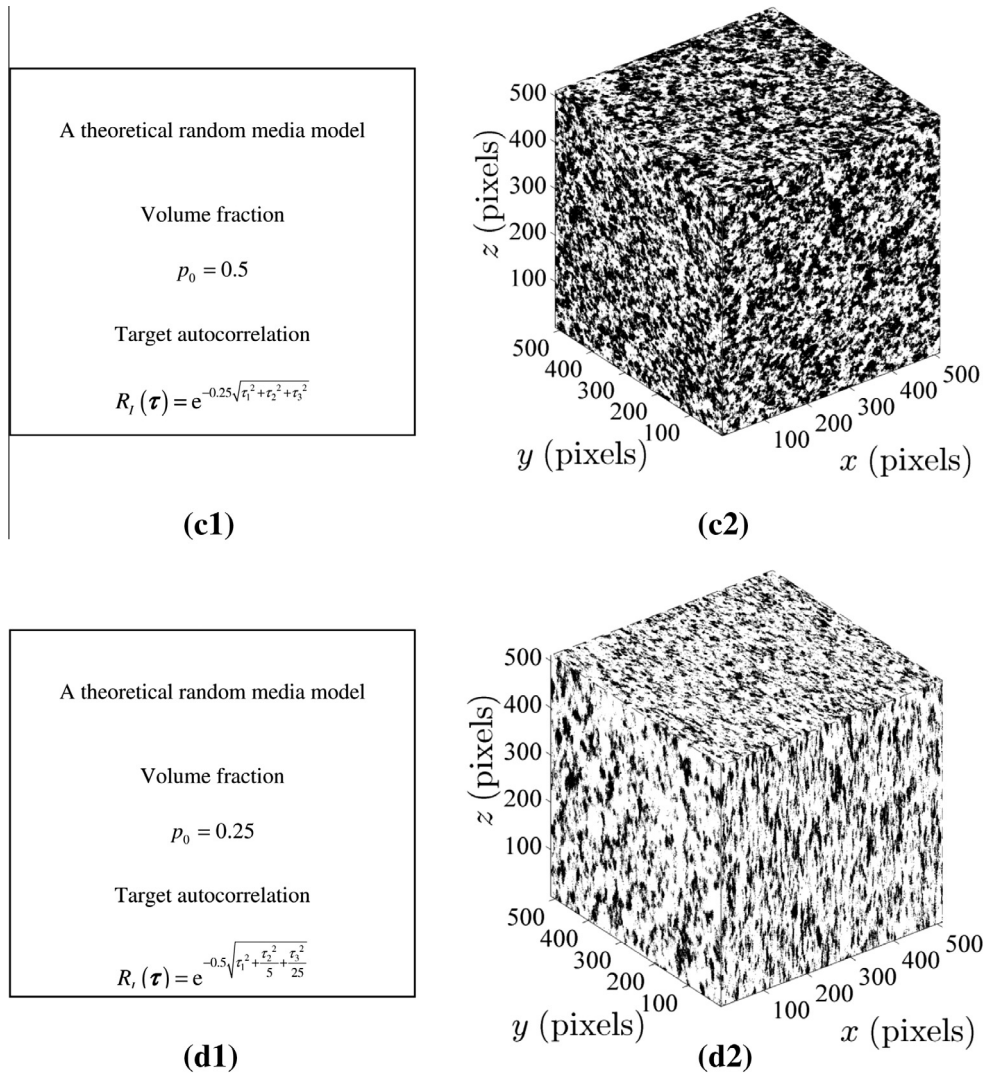


Fig. 10. (continued)

for the iterative nonlinear transformation method. The computational efficiencies for all three methods are listed in Table 1, in which the CPU time is recorded for the reconstruction of a single sample. It is noted that for multiple sample reconstruction, the total time cost will increase proportionally using the simulated annealing approach, while for the iterative nonlinear transformation method and the proposed method, the cost of additional sample reconstruction is negligible. It can be seen from Table 1 that the proposed method is significantly faster than existing methods. The very large efficiency improvement is due to the fact that the relationship between the target binary valued random field and the underlying Gaussian field is explicitly determined, such that the Gaussian fields and the associated random media samples can be directly reconstructed without costly iterations.

5.2. Two-dimensional random media reconstruction

Five 2D random media with different morphologies are considered in this example, and for comparison, they are reconstructed using the proposed and the simulated annealing method. The reconstruction results are shown in Fig. 8, in which the first column shows the reference random media, the second column shows the samples reconstructed with the proposed method, and the third column shows the de-noised samples reconstructed using the simulated annealing method. It can be seen that the new method is effective for the reconstruction of a wide range of random media with different morphologies. To examine the accuracy, the autocorrelations along the horizontal direction are shown on the left

Table 3 Performance data for 3D random media reconstruction.

Random media no.	a	b	c	d
3D media size (pixel × pixel × pixel)	512 × 512 × 512	512 × 512 × 512	512 × 512 × 512	512 × 512 × 512
p_0	0.5627	0.9222	0.5	0.25
CPU time cost (s)	27	27	27	27
Measured bounds of $R_l(\tau)$	[-0.1017,1]	[-0.0568,1]	(0, 1]	(0, 1]
Predicated compatibility bounds of $R_l(\tau)$	[-0.7772,1]	[-0.0844,1]	[-1, 1]	[-0.3333,1]

and the autocorrelations along the vertical direction are shown on the right. The autocorrelation comparison confirms that both the proposed method and the simulated annealing method can achieve good approximation to the target random media, while the proposed method exhibits slightly better accuracy. The reconstruction does have some limitations, causing small but visible differences between the original and the reconstructed media, which will be further investigated in Section 6.

The performance data of these 2D examples are listed in Table 2. For the proposed method, the CPU time listed in the table is the per-sample time cost averaged over 1000 sample reconstructions. For the simulated annealing method, the CPU time is recorded for a single sample reconstruction, and it will increase proportionally if multiple samples are reconstructed. It can be seen that the proposed method is four orders faster than the simulated annealing method. The volume fraction and the measured

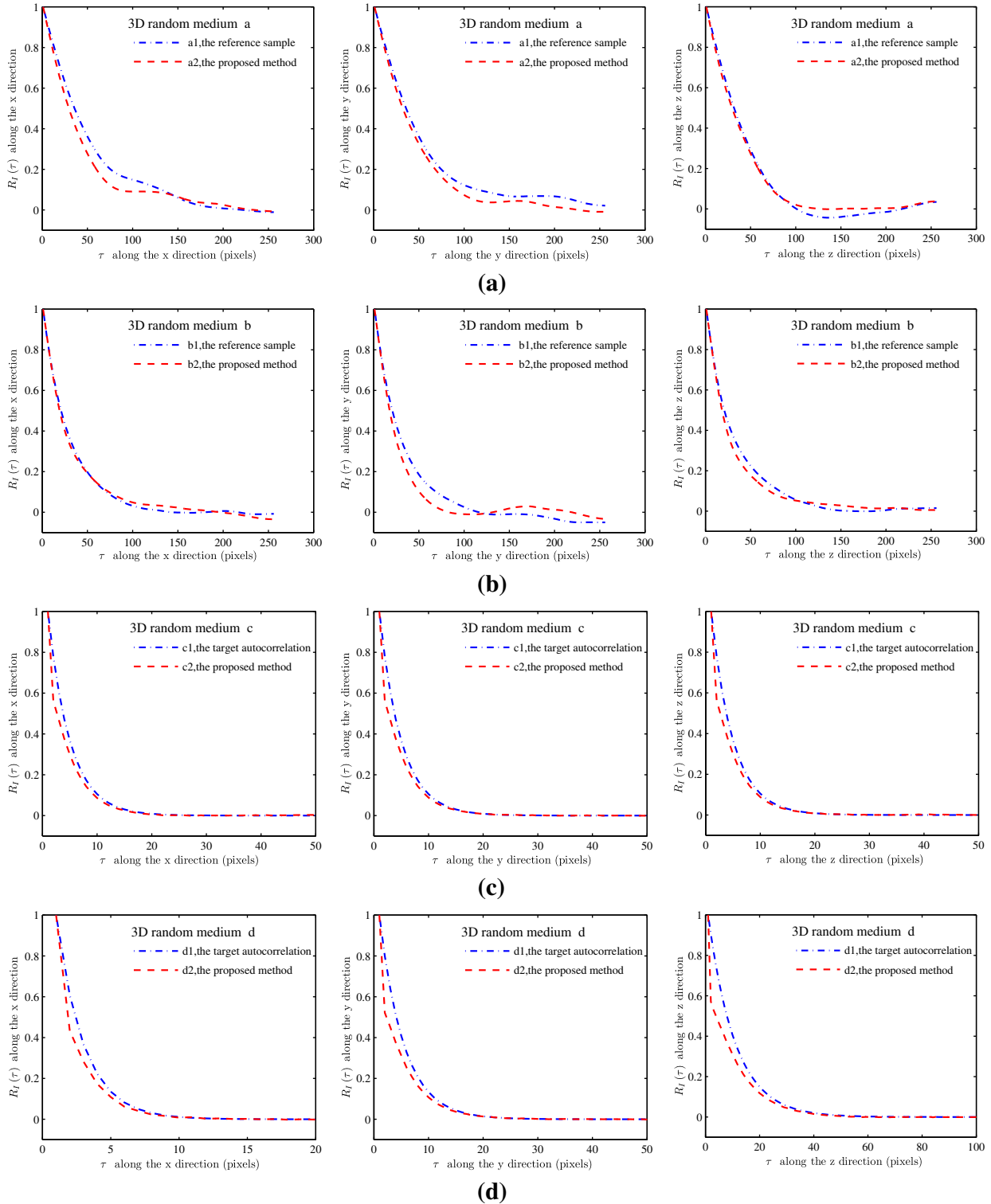


Fig. 11. Autocorrelation functions of the 3D random media samples in Fig. 10. Left: the autocorrelation along the x direction; center: the autocorrelation along the y direction; Right: the autocorrelation along the z direction.

autocorrelation function are also listed in the table together with the theoretical compatibility bound predicted by our method (see Eqs. (23), (24)). Given a reference random media sample, the predicted compatibility bounds allow a user to determine in prior whether samples can be reconstructed through nonlinear transformation of Gaussian fields, without tedious trial and error attempts.

5.3. Three-dimensional random media reconstruction

The benefits from the high computational efficiency of the proposed method can also be used to reconstruct large-size 3D random media samples. Statistical characteristics of a 3D random medium can be derived from its 2D slices [8,42–44]. Especially, if the 3D random medium is isotropic, a single 2D slice is sufficient to obtain all the statistical information required. Four random media samples are considered in this example, as shown in Fig. 10, where the reference random media are shown on the left and the corresponding reconstructed random media samples are shown on the right. Fig. 10(a) and (b) are samples of nuclear graphite Gilsocarbon [45], an isotropic graphite material with porous microstructure. Nuclear graphite Gilsocarbon is widely used as in-core structures of advanced gas-cooled reactors in the UK, and these 3D samples are obtained through three-dimensional X-ray scans. Fig. 10(c) and (d) are two theoretical random media models specified by their statistical characteristics, i.e. the volume fraction

and the autocorrelation function. The four reference random media samples have very different morphologies, and their volume fractions and autocorrelations are listed in Table 3. The reconstruction results shown in Fig. 10(e)–(h) demonstrate that the proposed method can successfully generate large-size 3D random media samples that conform to the given references.

The accuracy of the reconstruction is examined in Fig. 11 through the autocorrelation function. In Fig. 11, the first, second and last columns show the autocorrelation functions along the x-axis, y-axis and z-axis, respectively. A good reconstruction accuracy is observed in all four examples. The performance data are listed in Table 3. All four random media have the same size, $512 \times 512 \times 512$ pixels, and the sample is reconstructed in around 27 s. The measured bound of autocorrelation and the predicted compatibility bound are also listed in Table 3, and they can be used to determine a priori if the sample can be successfully reconstructed through the proposed method.

6. Limitation discussion

The first- and second- order statistical moments cannot completely characterize a general random field. Thus, the random media reconstructed using the proposed method can only be treated as an approximation of the original random medium sample, and they share the same statistical features measured by the expectation

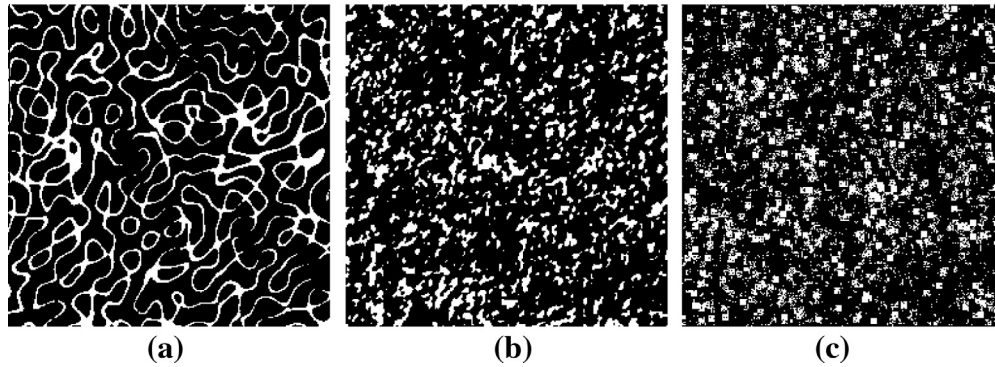


Fig. 12. A failure case for 2D random medium reconstruction. (a) The reference random medium sample; (b) a random medium sample reconstructed by the proposed method; (c) a random medium sample reconstructed by the simulated annealing method.

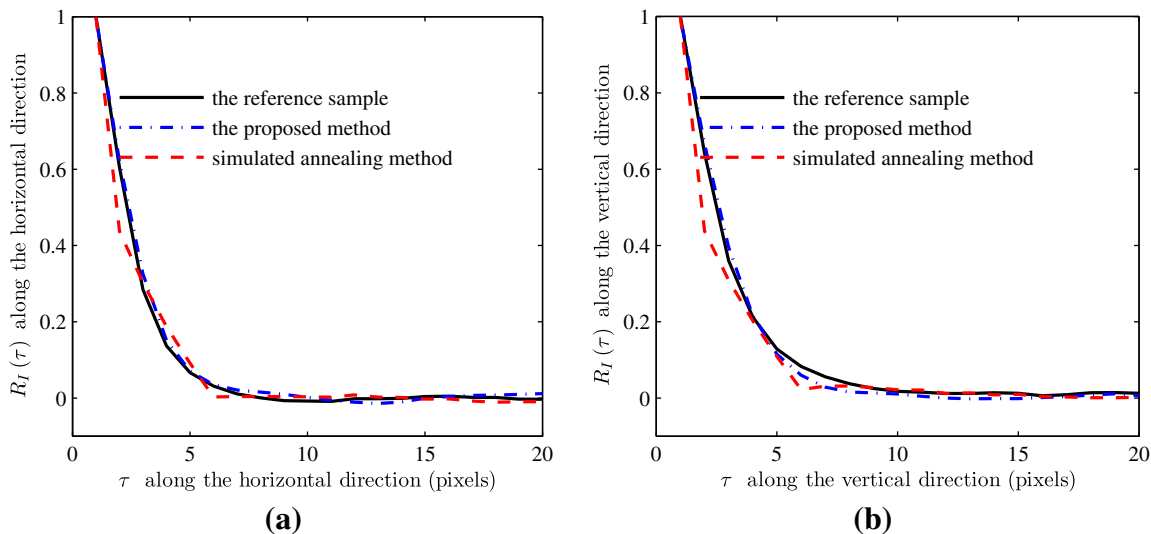


Fig. 13. Autocorrelation functions of the 2D random media in Fig. 12. (a) The autocorrelations along the horizontal direction; (b) the autocorrelations along the vertical direction.

and auto-correlation functions. We tested our method on a wide range of practical random media with different types of random patterns, and the proposed method is found to produce good reconstructions in most cases. However, failure cases are observed for random media with structured and continuous patterns. A typical failure case is shown in Fig. 12, where (a) is the reference medium sample and (b) and (c) are the reconstruction samples using the proposed method and the simulated annealing method respectively.

The reconstructed samples shown in Fig. 12(b) and (c) are clearly different from the original sample shown in Fig. 12(a). Measured by expectation, the volume fraction of all three samples are identical. To investigate the difference, we plot the autocorrelation functions in Fig. 13, where (a) shows the autocorrelation measured along the horizontal direction and (b) shows the autocorrelation measured along the vertical direction. It can be seen that all three samples have very similar second-order statistics. The reconstruction failed because the autocorrelation is not able to completely characterize a non-Gaussian field. Thus it is necessary to seek for other measures to identify the morphological difference among the three random media in Fig. 12.

Higher order statistics [46] is a category of methods for testing non-Gaussianity. One widely used higher order statistics measure is higher order moments [47], which are higher order generaliza-

tions of the first and second order statistical moments. The three-point correlation $R3_I(\tau_1, \tau_2)$ of the stationary real random field $I(\mathbf{x}, \omega)$ is defined as [48–50]:

$$R3_I(\tau_1, \tau_2) = \frac{E[(I(\mathbf{x}, \omega) - \mu)(I(\mathbf{x} + \tau_1, \omega) - \mu)(I(\mathbf{x} + \tau_2, \omega) - \mu)]}{E[(I(\mathbf{x}, \omega) - \mu)^3]}, \quad \forall \mathbf{x}, \quad (27)$$

where τ_1 and τ_2 are the relative displacements of the three points: \mathbf{x} , $\mathbf{x} + \tau_1$ and $\mathbf{x} + \tau_2$. Due to the stationary assumption, $R3_I(\tau_1, \tau_2)$ depends only on τ_1 and τ_2 , rather than \mathbf{x} . The three-point correlation is a third order statistical moment, and up to N -point correlation functions can be defined in a similar manner as Eq. (27).

To better examine the 2D random media in Fig. 12 using the three-point correlation $R3_I(\tau_1, \tau_2)$, we represent τ_1 and τ_2 in a polar coordinate system as (ρ_1, θ_1) and (ρ_2, θ_2) , where ρ_i denotes the distance to the origin and θ_i the angle measured from a fixed direction. For a direct graphical demonstration, the measured $R3_I(\tau_1, \tau_2)$ is only shown along some specific paths. Specifically, ρ_1, θ_1 and ρ_2 are fixed, while θ_2 is altered from 0° to 360° as shown in Fig. 14. The three-point correlations for all three samples in Fig. 12 are plotted in Fig. 15.

As shown in Fig. 15, the three samples in Fig. 12(a)–(c) exhibit distinct statistical features in the sense of three-point correlation. Non-negligible differences may also exist in other higher order correlations (e.g. 4-point correlation, 5-point correlation, etc.). The proposed method, utilizing only the marginal probability distribution (p_0) and the first two order moments, do not produce a unique and “exact” solution. The accuracy of the proposed method depends on how much information regarding the morphology are contained by the first two order moments. Higher order statistics offers a tool for detecting the information omitted by the first two order moments [48–51] and thus could be applied to make a rough judgement in advance for the reconstruction quality of the proposed method.

It is worth to note that higher order statistics is an active yet immature technique. The challenges of higher order statistics include: higher dimensions, requiring much more data, oversensitive to outliers. However, to efficiently incorporate higher order statistics for random media reconstruction is not within the scope of this paper.

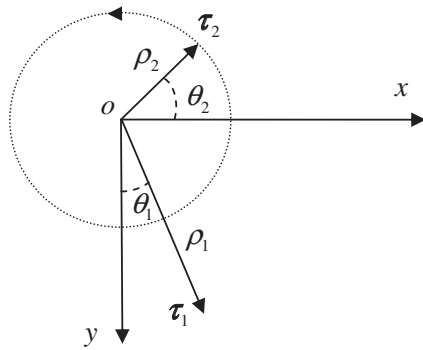


Fig. 14. A calculation path for three-point correlation under polar coordinate system.

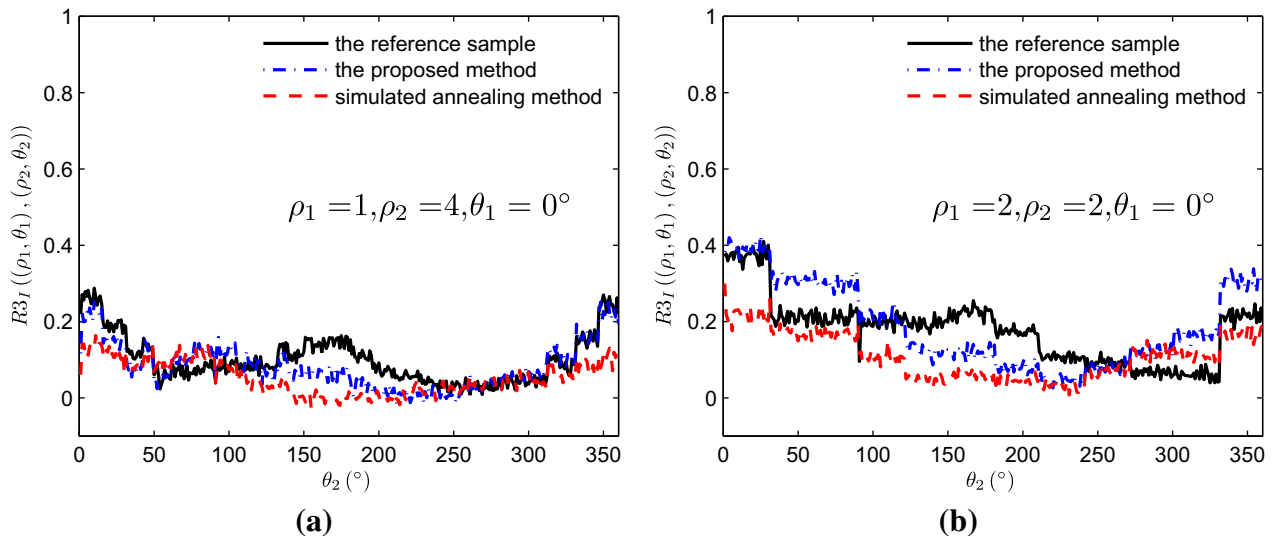


Fig. 15. Three-point correlations of the random media in Fig. 12. (a) Is computed along the path of $\rho_1 = 1, \rho_2 = 4$ and $\theta_1 = 0^\circ$, and (b) is computed along the path of $\rho_1 = 2, \rho_2 = 2$ and $\theta_1 = 0^\circ$.

7. Conclusion

A highly efficient method is developed for reconstructing two-phase composite materials with random morphology. It can be used for Monte Carlo simulations which require rapid reconstruction of large amounts of samples according to statistical characteristics derived from a few measured samples (reference samples). The new method is based on nonlinear transformation of Gaussian random fields. The explicitly reconstructed media are able to meet the binary-valued marginal probability distribution function and the two point correlation function of the reference media. The new method has the following advantages:

- It is thousands of times faster than the simulated annealing method, which is considered as the benchmark method for random media reconstruction. Unlike the simulated annealing method, where the simulation parameters need to be determined empirically (e.g. shape and size for pixel block exchange, annealing temperature and median filter et.), the proposed method is easy to implement and requires only the reference media sample as the input.
- Though the joint probability function of all points is needed to uniquely determine a random field, the marginal distribution plus covariance can offer considerable information for the morphology of practical random media. The proposed method shows sound reconstruction results for various types of 2D and 3D random media, as demonstrated by the examples.

It is possible to extend the proposed approach to multi-phase random media, for which the simulated annealing method is computationally prohibitive. It is also possible to combine the proposed method with other statistical reconstruction techniques to incorporate higher order statistical measures. These important aspects will be pursued in future work.

Acknowledgements

The authors would like to thank British Council and Chinese Scholarship Council for the support through the Sino-UK Higher Education Research Partnership for PhD Studies, the Royal Academy of Engineering for support from the Research Exchanges with China and Indian Award, the Natural Science Foundation of China (No. 11272181), and the Specialized Research Fund for the Doctoral Program of Higher Education of China (No. 20120002110080).

References

- [1] Yeong CLY, Torquato S. Reconstructing random media. *Phys Rev E* 1998;57:495–506.
- [2] Koutsourelakis PS, Deodatis G. Simulation of multidimensional binary random fields with application to modeling of two-phase random media. *J Eng Mech ASCE* 2006;132:619–31.
- [3] Patelli E, Schueller G. On optimization techniques to reconstruct microstructures of random heterogeneous media. *Comput Mater Sci* 2009;45:536–49.
- [4] Jeulin D. Random texture models for material structures. *Stat Comput* 2000;10:121–32.
- [5] Liu WK, Siad L, Tian R, Lee S, Lee D, Yin XL, et al. Complexity science of multiscale materials via stochastic computations. *Int J Numer Methods Eng* 2009;80:932–78.
- [6] Ostoja-Starzewski M. Random field models of heterogeneous materials. *Int J Solids Struct* 1998;35:2429–55.
- [7] Molchanov IS. *Theory of random sets*. Springer Verlag; 2005.
- [8] Yeong CLY, Torquato S. Reconstructing random media. II. Three-dimensional media from two-dimensional cuts. *Phys Rev E* 1998;58:224–33.
- [9] Jiao Y, Stillinger FH, Torquato S. Modeling heterogeneous materials via two-point correlation functions. II. Algorithmic details and applications. *Phys Rev E* 2008;77.
- [10] Graham-Brady L, Xu XF. Stochastic morphological modeling of random multiphase materials. *J Appl Mech Trans ASME* 2008;75.
- [11] Patelli E, Schueller GI. Computational optimization strategies for the simulation of random media and components. *Comput Optim Appl* 2012;1–29.
- [12] Sankaran S, Zabarar N. A maximum entropy approach for property prediction of random microstructures. *Acta Mater* 2006;54:2265–76.
- [13] Koutsourelakis PS. Probabilistic characterization and simulation of multi-phase random media. *Prob Eng Mech* 2006;21:227–34.
- [14] Kindermann R, Snell JL, Society AM. *Markov random fields and their applications*. American Mathematical Society Providence, RI; 1980.
- [15] Jaynes ET. Information theory and statistical mechanics. *Stat Phys Brandeis Lect* 1963;3:160–85.
- [16] Jaynes ET. Information theory and statistical mechanics. II. *Phys Rev* 1957;108:171.
- [17] Gilks WR, Richardson S, Spiegelhalter DJ. *Markov chain Monte Carlo in practice*. Chapman & Hall/CRC; 1996.
- [18] Metropolis N, Rosenbluth AW, Rosenbluth MN, Teller AH, Teller E. Equation of state calculations by fast computing machines. *J Chem Phys* 1953;21:1087.
- [19] Chib S, Greenberg E. Understanding the metropolis-hastings algorithm. *Am Stat* 1995;327–35.
- [20] Geyer CJ, Thompson EA. Annealing Markov chain Monte Carlo with applications to ancestral inference. *J Am Stat Assoc* 1995:909–20.
- [21] Song PXX. Multivariate dispersion models generated from Gaussian copula. *Scand J Stat* 2000;27:305–20.
- [22] Grigoriu M. Simulation of stationary non-Gaussian translation processes. *J Eng Mech ASCE* 1998;124:121–6.
- [23] Roberts AP, Teubner M. Transport properties of heterogeneous materials derived from Gaussian random fields: bounds and simulation. *Phys Rev E* 1995;51:4141–54.
- [24] Berk NF. Scattering properties of the leveled-wave model of random morphologies. *Phys Rev A* 1991;44:5069–79.
- [25] Yamazaki F, Shinozuka M. Digital generation of non-Gaussian stochastic fields. *J Eng Mech ASCE* 1988;114:1183–97.
- [26] Deodatis G, Micaletti RC. Simulation of highly skewed non-Gaussian stochastic processes. *J Eng Mech ASCE* 2001;127:1284–95.
- [27] Popescu R, Deodatis G, Prevost JH. Simulation of homogeneous nonGaussian stochastic vector fields. *Prob Eng Mech* 1998;13:1–13.
- [28] Shields MD, Deodatis G, Bocchini P. A simple and efficient methodology to approximate a general non-Gaussian stationary stochastic process by a translation process. *Prob Eng Mech* 2011;26:511–9.
- [29] Grigoriu M. Existence and construction of translation models for stationary non-Gaussian processes. *Prob Eng Mech* 2009;24:545–51.
- [30] Grimmett GR, Stirzaker DR. *Probability and random processes*. 3 ed. Oxford: Oxford university press; 2001.
- [31] Priestley MB. *Spectral analysis and time series*. London: Academic Press; 1981.
- [32] Koopmans LH. *The spectral analysis of time series*. Academic Press; 1995.
- [33] Mallat SG. *A wavelet tour of signal processing*. Academic Press; 1999.
- [34] Li CF, Feng YT, Owen DRJ, Davies IM. Fourier representation of random media fields in stochastic finite element modelling. *Eng Comput* 2006;23:794–817.
- [35] Li CF, Feng YT, Owen DRJ, Li DF, Davis IM. A Fourier-Karhunen-Loeve discretization scheme for stationary random material properties in SFEM. *Int J Numer Methods Eng* 2008;73:1942–65.
- [36] Higham NJ. Computing the nearest correlation matrix – a problem from finance. *IMA J Numer Anal* 2002;22:329–43.
- [37] Qi HD, Sun DF. A quadratically convergent Newton method for computing the nearest correlation matrix. *SIAM J Matrix Anal Appl* 2006;28:360–85.
- [38] Borsdorf R, Higham NJ. A preconditioned Newton algorithm for the nearest correlation matrix. *IMA J Numer Anal* 2010;30:94–107.
- [39] Beauchamp KG, Yuen C. *Digital methods for signal analysis*. London: Routledge; 1979.
- [40] Shanmugan KS, Breipohl AM. *Random signals: detection, estimation, and data analysis*. New York: John Wiley & Sons; 1988.
- [41] Otne RK, Enochson L. *Applied time series analysis*. New York: John Wiley & Sons; 1978.
- [42] Roberts AP. Statistical reconstruction of three-dimensional porous media from two-dimensional images. *Phys Rev E* 1997;56:3203–12.
- [43] Talukdar MS, Torsæter O, Ioannidis MA. Stochastic reconstruction of particulate media from two-dimensional images. *J Colloid Interface Sci* 2002;248:419–28.
- [44] Ioannidis MA, Chatzis I. On the geometry and topology of 3D stochastic porous media. *J Colloid Interface Sci* 2000;229:323–34.
- [45] Wang HT, Hall G, Yu SY, Yao ZH. Numerical simulation of graphite properties using X-ray tomography and fast multipole boundary element method. *CMES Comput Model Eng Sci* 2008;37:153–74.
- [46] Stuart A, Ord K. *Kendall's advanced theory of statistics: distribution theory*. 6 ed. London: Charles Griffin; 1994.
- [47] Lukacs E. *Characteristic functions*: Griffin London 1960.
- [48] Mendel JM. Tutorial on higher-order statistics (spectra) in signal-processing and system-theory – theoretical results and some applications. *Proc IEEE* 1991;79:278–305.
- [49] Nikias CL, Raghuveer MR. Bispectrum estimation – a digital signal-processing framework. *Proc IEEE* 1987;75:869–91.
- [50] Nikias CL, Mendel JM. Signal processing with higher-order spectra. *IEEE Signal Process Mag* 1993;10:10–37.
- [51] Collis WB, White PR, Hammond JK. Higher-order spectra: the bispectrum and trispectrum. *Mech Syst Signal Process* 1998;12:375–94.